DTU Library

Unveiling PET Hydrolase Surface Dynamics through Fluorescence Microscopy

Rennison, A. P.; Nousi, A.; Westh, P.; Marie, R.; Møller, M. S.

Published in:
ChemBioChem

Link to article, DOI:
10.1002/cbic.202300661

Publication date:
2024

Document Version
Publisher's PDF, also known as Version of record

ChemBioChem

Research Article
doi.org/10.1002/cbic.202300661

Chemistry Europe
European Chemical Societies Publishing

www.chembiochem.org

Unveiling PET Hydrolase Surface Dynamics through Fluorescence Microscopy

A. P. Rennison+,[a] A. Nousi+,[b] P. Westh,*[a] R. Marie,*[b] and M. S. Møller*[a]

PET hydrolases are an emerging class of enzymes that are being heavily researched for their use in bioprocessing polyethylene terephthalate (PET). While work has been done in studying the binding of PET oligomers to the active site of these enzymes, the dynamics of PET hydrolases binding to a bulk PET surface is an unexplored area. Here, methods were developed for total internal reflection fluorescence (TIRF) microscopy and fluorescence recovery after photobleaching (FRAP) microscopy to study the adsorption and desorption dynamics of these proteins onto a PET surface. TIRF microscopy was employed to measure both on and off rates of two of the most commonly studied PET hydrolases, PHL7 and LCC, on a PET surface. It was found that these proteins have a much slower off rates on the order of 10^{-3} s^{-1}, comparable to non-productive binding in enzymes such as cellulose. In combination with FRAP microscopy, a dynamic model is proposed in which adsorption and desorption dominates over lateral diffusion over the surface. The results of this study could have implications for the future engineering of PET hydrolases, either to target them to a PET surface or to modulate interaction with their substrate.

Introduction

Enzymatic hydrolysis of synthetic polymers has been a subject of research for over a decade,[1] with a particular focus on enzymatic recycling of polyethylene terephthalate (PET).[2,3] Now it has the potential to become a mature industrial process.[4] Most recent studies in enzymatic PET hydrolysis have focused on cutinases, such as the leaf-branch compost cutinase (LCC),[5] or the polyester hydrolase 7 (PHL7),[6] both of which were discovered from metagenomics studies. While these enzymes, and associated variants, do have some significant activity on amorphous PET, more work is still needed in engineering them to exhibit activity on crystalline PET, as well as at lower temperatures. Understanding the processes by which these cutinases perform interfacial catalysis is therefore essential to the further development of enzymatic bioprocessing of PET.

[a] A. P. Rennison,+ P. Westh, M. S. Møller
Department of Biotechnology and Biomedicine,
Technical University of Denmark,
2800 Kongens Lyngby, Denmark
E-mail: petwe@dtu.dk
msmo@dtu.dk

[b] A. Nousi,+ R. Marie
Department of Health Technology,
Technical University of Denmark,
2800 Kongens Lyngby, Denmark
E-mail: rcwm@dtu.dk

[+] These authors contributed equally.

Supporting information for this article is available on the WWW under https://doi.org/10.1002/cbic.202300661

The study and engineering of PET hydrolases has so far generally focused on active site architecture and improvements to enzyme thermostability.[4,7,8] While activity of the enzymes overall has been increased, relatively little attention has been paid to the adsorption of the PET hydrolases to the insoluble surface of the substrate. The dynamics of enzyme adsorption and desorption during interfacial catalysis has been shown to be vital to degradation of insoluble polysaccharides such as cellulose,[9] and the same is to be expected of PET hydrolysis. Some attempts to engineer PET hydrolases from the viewpoint of surface adsorption have been made, including the addition of substrate binding modules.[10,11] However, the dynamics of these systems remain largely unexplored.

The binding of PET hydrolases to PET has been quantified with most enzymes showing a surprisingly high affinity for the substrate, with dissociation constants (K_d) in the low nM range.[12] It has also been shown that a lower affinity can actually have a positive effect on the activity of the enzymes, with LCC showcasing lower affinity yet higher activity than other cutinases.[13,14] However, increased affinity originating from fusion of carbohydrate-binding modules (CBMs) to PET hydrolases can improve activity,[15] at least at low substrate loadings. These results suggest that the dynamics of adsorption and desorption to the insoluble surface are key to high activity, and warrant further investigation.

Enzyme dynamics during interfacial catalysis can studied using fluorescence imaging techniques, such as Total Internal Reflection Fluorescence (TIRF) microscopy and Fluorescence Recovery After Photobleaching (FRAP) microscopy. TIRF microscopy is a single-molecule imaging technique.[16] It operates by exciting fluorescently labeled molecules at a glass-water interface, utilizing an evanescent field that decays exponentially into the solution. Typically the sample is deposited on the glass surface and the decay length is approximately

100 nm. The exponentially decaying excitation causes the rejection of background signal, providing a high signal-to-noise ratio. This allows for the detection of single molecule adsorption to the surface of thin materials. TIRF has been used to study the interfacial surface dynamics of the cellulase Cel7A from the cellulolytic fungus *Trichoderma reesei*,[17–20] along with the proteolytically isolated catalytic domain and CBM from the full-length enzyme. Dissociation rate constants (k_{OFF}) and association rate constants (r_{ON}) of the proteins onto the insoluble surface of the substrate can be measured, and related to activity.[17,21] FRAP microscopy is a well-established technique in which fluorescently labeled proteins on a surface can be bleached by a high-powered excitation laser, after which the surface dynamics can be studied as the fluorescence is recovered from proteins diffusing over the surface. This has been used to measure diffusion rates of fluorescently labeled cellulases from *Cellulomonas fimi* over a cellulose surface.[22] FRAP allows for determination of diffusion rates of proteins over a surface, as well as an estimation of k_{ON} and k_{OFF}, providing a complimentary method to TIRF in studying the dynamics of proteins in interfacial catalysis.

In this study, several different approaches have been used to study the dynamics of PET hydrolases on PET, as shown in Figure 1. Fusion proteins have been produced between super-folder green fluorescent protein (*sf*GFP) and the two industrially relevant PET hydrolases PHL7 and the LCC variant LCC^{ICCG},[4] both with and without a PET binding family 2 CBM.[23] K_d of each protein on PET have been determined from langmuir adsorption isotherms, and activity of all the fusion enzymes on PET discs has been assayed. Both TIRF and FRAP microscopy have been used to investigate the surface dynamics of these PET hydrolases on a PET surface. It is to the knowledge of the authors the first report of dynamic rates of diffusion, adsorption and desorption in these systems. Given the lack of knowledge of surface dynamics of PET hydrolases, such kinetics data is highly relevant information for the future engineering of PET hydrolases, and bioprocessing of synthetic plastics in general.

Results and Discussion

Protein Constructs Produced

Six different protein constructs were designed, expressed and purified in this study, as outlined in Figure 1a. These included two of the most commonly studied PET hydrolases, LCC^{ICCG} and PHL7, both with and without the PET binding *Ba*CBM2 module. Furthermore, all protein constructs except *sf*GFP alone had a C-terminal StrepII tag to allow for determination of bleaching time of *sf*GFP, when it is fused with other proteins. Protein sequences of each construct can be found in the Supporting Information note N1.

PET Hydrolase Activity of *sf*GFP Labelled Enzyme Constructs

Prior to the study of the surface dynamics of PET hydrolases fused to *sf*GFP, it was investigated whether this fusion affected the activity of the PET hydrolases. To this end, activity assays were performed on each construct that contained either the LCC^{ICCG} or PHL7 modules (Figure 1a), and compared these to the activity of the unlabelled enzymes (Figure 2). Each of the *sf*GFP labeled enzymes maintained activity. Both *sf*GFP-LCC^{ICCG} and *sf*GFP-PHL7 showed a reduced activity when compared to their unlabelled analogs, potentially suggesting that the large *sf*GFP module affects the binding of catalytic domains to the PET, which is then recovered by the addition of the *Ba*CBM2 module. Nevertheless, the comparable activity of all of the labeled enzymes with their unlabeled analogs shows that the hydrolytic domains in each of these proteins are correctly folded and active, and we can consider that the *sf*GFP labelled enzymes have similar kinetic parameters to the wild type proteins.

Affinity of *sf*GFP Labelled Constructs for PET

PET hydrolases are known to have a high affinity for the PET, with K_d values often in the tens of nM.[12] In order to address the binding affinities of the enzymes labeled with *sf*GFP, steady-state binding assays (Figure 1b) using the fluorescent signal for detecting the low concentrations of unbound protein at high affinities were performed (Table 1).

Each of the proteins assayed shows a high affinity for the amorphous PET discs, with each K_d being in the low to medium nM range (Table 1). The adsorption of proteins and short peptides to plastics is a known phenomenon that has been studied for many years in an effort to reduce protein loss in laboratory plastic ware.[24,25] However, some differences can be seen between the different proteins. *sf*GFP-*Ba*CBM2 shows the highest affinity for the plastic, which is to be expected given the known specific affinity of such Type A CBMs for insoluble hydrophobic substrates.[23,26] It should also be stated that *sf*GFP has a similar affinity for the amorphous PET as the PET hydrolase enzymes. This is expected from previous studies of proteins adsorption to plastics.[25] However, as an affinity change can be measured upon the addition of different binding modules onto the *sf*GFP module, there was con-

Table 1. Binding parameters, K_d and B_{max}, of proteins on amorphous PET discs. Each assay was performed at 20 °C, in duplicates. Individual binding isotherms can be found in Figure S1.

Protein	K_d (nM)	B_{max} (nmol/cm^2)
*sf*GFP-LCC^{ICCG}	67.9 ± 7.1	0.065 ± 0.005
*sf*GFP-LCC^{ICCG}-*Ba*CBM2	28.2 ± 3.6	0.043 ± 0.001
*sf*GFP-PHL7	289.8 ± 84.4	0.129 ± 0.017
*sf*GFP-PHL7-*Ba*CBM2	39.3 ± 8.2	0.021 ± 0.004
*sf*GFP-*Ba*CBM2	30.8 ± 6.6	0.021 ± 0.003
*sf*GFP	256.2 ± 2.7	0.069 ± 0.003

Chemistry Europe
European Chemical Societies Publishing

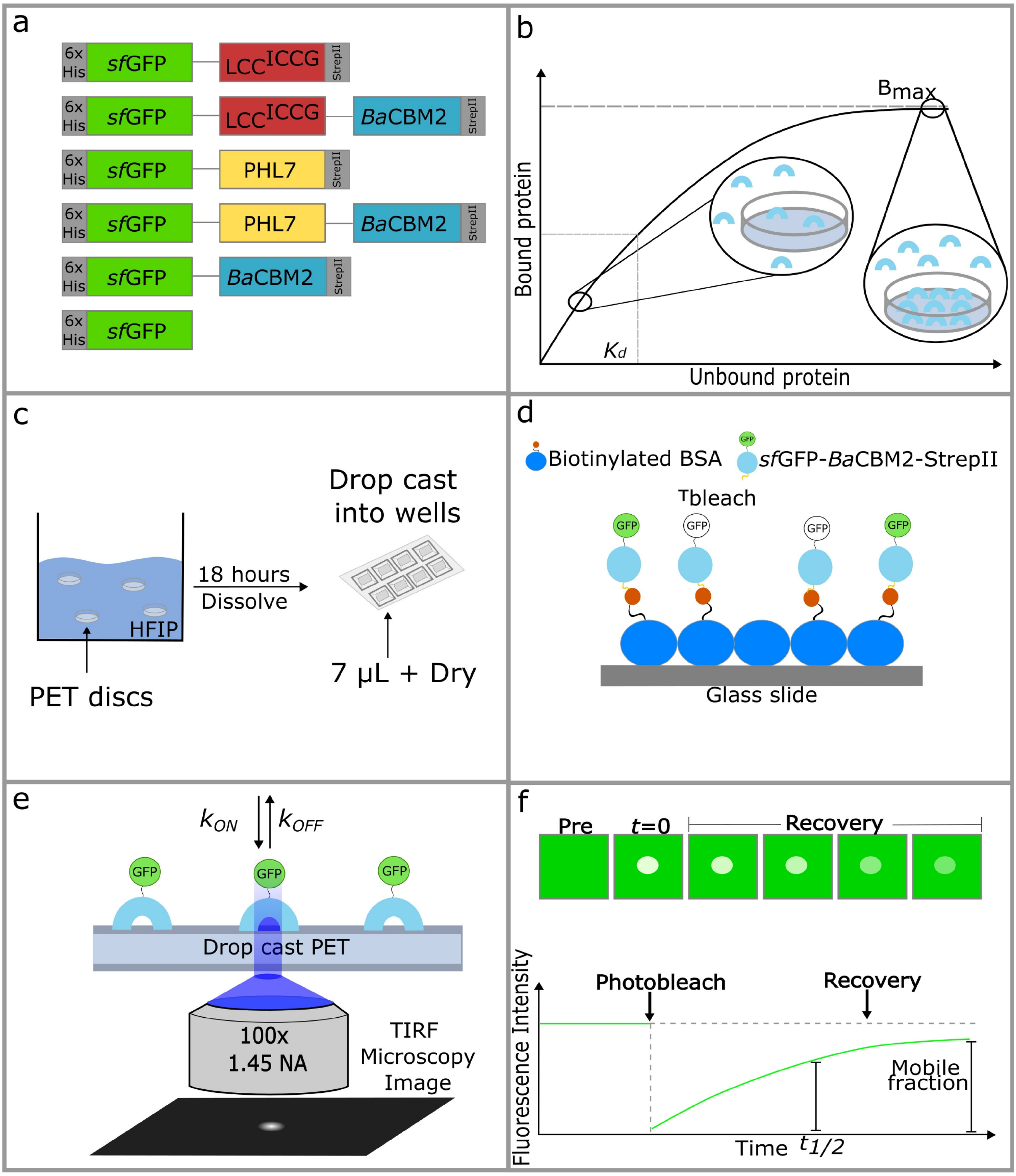

Figure 1. Overview of experimental procedures performed in this study. a) An overview of the protein constructs produced. b) Steady state adsorption assays. c) Drop casting of PET onto glass slides for use in TIRF microscopy. d) Determination of the photobleaching time of *sf*GFP using a single-molecule assay. e) Single-molecule experiments with TIRF microscopy for determination of PET hydrolase kinetic parameters. f) FRAP assays for determination of the type of bulk dynamics displayed by PET hydrolases.

fidence in the measurement of the binding of the PET hydrolases and CBMs rather than only the *sf*GFP. Furthermore, there is close agreement in the K_d values on PET of each of the enzymes when assayed without a *sf*GFP module despite using PET powder instead of PET film with the non-*sf*GFP labelled enzymes (Figure S2 and Table S1).

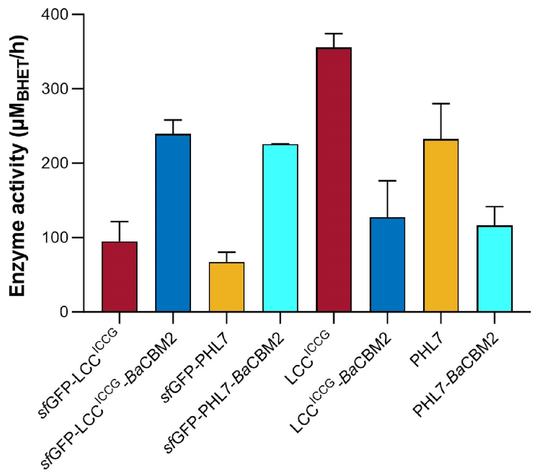

Figure 2. Activity of the *sf*GFP labelled PET hydrolases used in this study, along with their unlabelled analogs. Assays were performed on amorphous PET discs at 65 °C. Error bars represent the standard deviation between three replicates.

The maximum specific binding (B_{max}) of each of the proteins are similar, apart from the case of *sf*GFP-PHL7, which has a B_{max} approximately double that of *sf*GFP-LCC^{ICCG} (Table 1). The B_{max} may be viewed as the capacity of each disc to hold protein, suggesting that the PHL7 enzyme has a more efficient packing capability than the other enzymes. PHL7 has a negatively charged patch on one side of the enzyme, implying potential repulsion from the partial negative charge on a PET surface.[27] This could facilitate a more orderly protein arrangement on the surface, with the same face of the enzyme binding to the PET. Consequently, it allows for an increased capacity of protein binding to the plastic surface.

Characteristics of PET Film Used for TIRF Microscopy

TIRF microscopy was used to perform a single molecule analysis of each of the *sf*GFP labeled proteins expressed in the study (Figure 1a), along with a commercial GST-*sf*GFP control protein, on a PET surface. To this end a thin PET film was deposited onto a glass surface of an 8-well plate (Figure 1c). Total internal reflection illumination is typically obtained at the glass-to-water interface however here it is noted that due to the high refractive index of PET compared to glass, the exponentially decaying evanescent field extends from the PET surface into the solution. The PET formed a thin film on the surface of the microscopy glass slide, often with discontinuities (Figure S3a). Such areas were avoided for imaging, in an effort to keep the density of PET similar between experiments. During the course of the TIRF experiments, it was observed that PET itself has a noticeable autofluorescence (Figure S3b) in the 473 nm laser excitation used for the TIRF imaging of the *sf*GFP-labelled enzymes.

Establishment of *sf*GFP and PET Autofluorescence Photobleaching Times for TIRF Microscopy Analysis

In implementing the TIRF microscopy method, a photobleaching assay was conducted to analyze the photophysics of the *sf*GFP label (Figure 1d and Figure S4). Differentiating between enzyme dissociation and fluorophore photobleaching in single-molecule imaging is crucial, as both events result in a fluorescent spot that no longer emits. Establishing the bleaching time enables this distinction. A sufficiently extended photobleaching time, surpassing the enzyme residence time, strongly indicates that disappearing spots result from enzyme dissociation, leading to a residence time calculation with high certainty. The bleaching time of a single fluorophore molecule is a relevant parameter only in single-molecule studies, such as the TIRF assay, and is not applicable to the FRAP assay (see section FRAP Microscopy). In TIRF assays, the goal is to prolong the fluorophore bleaching time for precise measurements of the dissociation constant. Conversely, in FRAP assays, fluorophores are rapidly bleached to facilitate measurements of the recovery half time $t_{1/2}$. In TIRF and FRAP microscopy, the resolution of the image is limited by diffraction, typically around 250 nm, corresponding to approximately half the wavelength of the emitted light. In TIRF we operate at low molecule density (see section Processing of TIRF microscopy data) so individual molecules appear as isolated diffraction-limited spots approximately 250 nm in diameter. For FRAP microscopy proteins are imaged at high concentrations, precluding the observation of individual molecules.

The photobleaching assay was performed on a BSA-biotin coated glass surface with *sf*GFP-*Ba*CBM2 immobilized via a StrepII tag. This immobilization setup ensures that the observed signal reduction is specifically due to the photobleaching of *sf*GFP, rather than protein dissociation from the surface, as would occur with a PET surface. The bleaching time of the fluorescent module was determined under imaging conditions employed for the remainder of the study. After image acquisition, the fluorophore intensity tracks over time was loaded into Matlab (See Supporting Information note N2). The script used a maximum likelihood estimator and fitted the time traces to determine the decay times for each fluorophore (see Figure S4a). The acquired decay times were then plotted into histograms that were well described (p-value >0.05) by a single exponential decay (Figure S5) from which the mean bleaching time τ_{bleach} was estimated to be 70 ± 2 seconds under the specified imaging conditions.

The PET exhibited significant autofluorescence (Figure S3). To minimize this, before introducing the protein in each imaging session, the PET autofluorescence was reduced by increasing the laser power and illuminating the chosen PET FOV. This process facilitated the bleaching of spurious autofluorescence spots. However, complete removal of autofluorescence was not achieved, and some spots persisted. Therefore, the mean duration of PET autofluorescence spots ($\tau_{background}$) was assessed using measurements of PET background without protein. This assessment was crucial for accounting for autofluorescence during the data analysis of

Research Article
doi.org/10.1002/cbic.202300661

binding assays. The extracted duration of autofluorescence events was represented in a histogram (see Figure S4a). This was well-fitted (p-value >0.05) by a single exponential decay and $\tau_{background}$ was found to be 10.3 ± 0.5 seconds.

PET Hydrolase Association and Dissociation Rate Constants Measured Using TIRF Microscopy

Following the initial determinations of substrate autofluorescence and photo-bleaching of the *sf*GFP label, the kinetics of the PET hydrolases binding to the PET surface were assessed using single-molecule TIRF microscopy (Figure 1e). *sf*GFP-LCC^{ICCG} and *sf*GFP-PHL7, both with and without the *Ba*CBM2 module were imaged, along with *sf*GFP-*Ba*CBM2, *sf*GFP, and commercial GST-*sf*GFP. The characteristic bleaching time of the *sf*GFP and the acquired spot lifetimes for each protein were found to be of the same order of magnitude. Consequently, it was necessary to take the photobleaching time into account before calculating the residence times of the enzymes and the corresponding k_{OFF} values, using the spot lifetime τ_{meas}. The spot lifetime is acquired as the minimum of two events: the fluorophore photobleaching or the enzyme dissociating. The inverse of the residence time (τ_{res}) can be expressed as the difference between the inverse of spot lifetime (τ_{meas}) and the inverse of the bleaching time (τ_{bleach}), $1/\tau_{res} = 1/\tau_{meas} - 1/\tau_{bleach}$ (See Supporting Information note N3). Therefore, each characteristic spot lifetime acquired through fitting (Figure 3a) was modified to also take into account the *sf*GFP bleaching time. Taking the inverse of τ_{res} results in the k_{OFF} for each enzyme. Furthermore, the number of new binding events observed in each frame have been plotted over time. This analysis allows extraction of the molar binding rate constant of the enzyme, denoted as r_{ON} in $pM^{-1} s^{-1}$ (Figure 3b).

The histograms of spot lifetimes measured for the enzymes were well described by double exponential decays which would indicate two populations of binding events. However, the first population consistently throughout the experiments had a characteristic time of about 10 seconds, which is comparable to the PET background fluorescence $\tau_{background}$, which was measured on the PET film alone. The similarity in decay times (10 seconds) of the autofluorescence and the initial phase of the biexponential decay suggests that the first exponential results from lingering autofluorescent spots decaying during enzyme imaging. This interpretation is further bolstered by our photobleaching experiments, where GFP decay was adequately fit by a single exponential (p-value >0.5), ruling out a second characteristic GFP decay time. Alternatively, the initial decay could be attributed to short-lived GFP-module binding to the PET substrate before diffusing back into solution. Based on these considerations, we conclude that the first exponential decay is not indicative of enzyme binding/unbinding and is therefore excluded from our analysis and the long-lasting spots were used to measure the residence time.

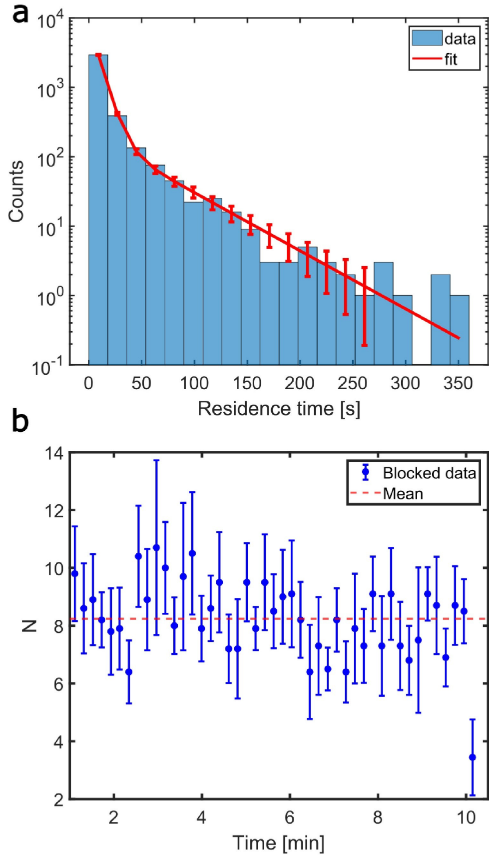

Figure 3. Residence time and binding rate analysis of PET degrading enzymes. a) An example of a histogram of spot duration as acquired from the time-lapse stacks of measurements done with the *sf*GFP-LCC^{ICCG} construct, as well as the double exponential fit (red) to it for the derivation of the residence time of the enzymes on PET. Error bars are the $\sqrt{N}$ of the expected number of counts in each bin. b) Example of the average number of new binding events of *sf*GFP-LCC^{ICCG} blocked per 10 frames in a single time-lapse movie. The data are well described by the average of new binding events. The error bars represent the standard error of the mean (s.e.m).

The residence time and k_{OFF} findings rest on a robust methodology. Efficient bleaching of PET resulted in reduced background noise, improving single-molecule spot analysis precision. Analyzing numerous spots enhanced statistical validity. Furthermore, histogram data aligned with the biexponential models, as confirmed by chi-squared goodness-of-fit tests (significance level $\alpha = 0.05$) and p-values $= 0.2$–0.9, confirming the results' accuracy. The reliability of the residence time calculation is further solidified by the robust and innovative mathematical correction implemented (refer to Supporting Information note N3) for the photophysics of the fluorescent probe. This methodological approach, grounded in established statistical analysis, ensures the precision of residence time calculations even in scenarios where bleaching times are comparable to or shorter than the lifetimes of the fluorescent spots.

After correcting for the bleaching time of the *sf*GFP, the residence times of each of the proteins was measured in the range of 200 to 400 seconds (see Table S2), which is generally much longer than the productive residence times seen in experiments performed with cellulase enzymes on cellulose fibrils. For example, Mudinoor *et al.*[17] report two types of binding events for Cel7A, with the short productive one being around 15 seconds. Haviland *et al.*[19] also report that Cel7A molecules conjugated with quantum dots exhibited static binding with duration of approximately 89 seconds and processive binding of 166 seconds. Moreover, Jung *et al.*[28] also report a double exponential behavior of cellulase molecules, with approximate durations of 30 and 173 seconds, giving an average of 53 seconds. Within the group of spots identified as enzymes rather than autofluorescence, only one population of bound enzymes was seen during these experiments. This compares to the productive low residence times, which can be suggested as specific binding, and nonproductive high residence times, assumed as non-specific, seen with Cel7A binding to cellulose. This is an indication that the binding exhibited by the enzymes in this work is nonspecific, likely due to the fact that the enzymes are being used on a non-natural substrate, as compared to the dual specific and nonspecific binding modes present in the fully evolved cellulolytic system. The non-specific binding of some PET hydrolases to a PET surface has been demonstrated before in biochemical assays,[12] which can be reasonably assumed to also be the case for LCC^{ICCG} and PHL7.

When comparing the dissociation rate constants (inverse of the corrected residence time) of the different enzymes, there are also some interesting differences (Figure 4a). The PET hydrolases generally have a lower k_{OFF} than *sf*GFP and GST-*sf*GFP, on average $k_{OFF} = 0.003 \pm 0.001\ s^{-1}$ (red line in Figure 4a). However, *sf*GFP-LCC^{ICCG} has a higher k_{OFF} compared to the other PET hydrolases, itself being similar to the two proteins without activity on PET. Their k_{OFF} is on average $k_{OFF} = 0.005 \pm 0.001\ s^{-1}$ (blue line in Figure 4a), exhibiting a significant difference with the rest of the hydrolases. LCC^{ICCG} is generally seen as the leading PET hydrolase in industry,[4] due to high thermostability and activity compared to other enzymes such as PHL7. The shorter residence time of LCC^{ICCG} compared to PHL7 could explain its higher overall activity, considering that an enzyme that adsorbs and desorbs efficiently from a surface is recruited faster to a new attack site. This has also been suggested previously when comparing LCC^{ICCG} to other PET hydrolases, in accordance with the Sabatier principle, which states that the optimum activity of a protein often occurs when an enzyme has an intermediate affinity, being neither adsorption or desorption limited.[14] It has also been recently shown that the two enzymes produce markedly different degradation profiles on a PET surface,[27] with PHL7 producing a crater-like effect on the surface, whereas LCC^{ICCG} produces a smoother surface upon degradation. This observation could also be due to the longer residence time of PHL7 compared to LCC^{ICCG}, as the longer an enzyme spends in one position, the more likely it is to bore into the surface.

For LCC^{ICCG}, fusion of the *Ba*CBM2 module led to a reduced k_{OFF} (Figure 4a; Table 2), with *sf*GFP-LCC^{ICCG}-*Ba*CBM2 having a value approximately half of *sf*GFP-LCC^{ICCG}. This is not surprising, given that type A CBM modules are known to have a specific binding surface for insoluble hydrophobic surfaces,[23] which could lead to a slower dissociation. *Ba*CBM2 also seems to hinder the mobility of the proteins since it lowers the molar binding rate constant r_{ON}, with both *sf*GFP-PHL7-*Ba*CBM2 and

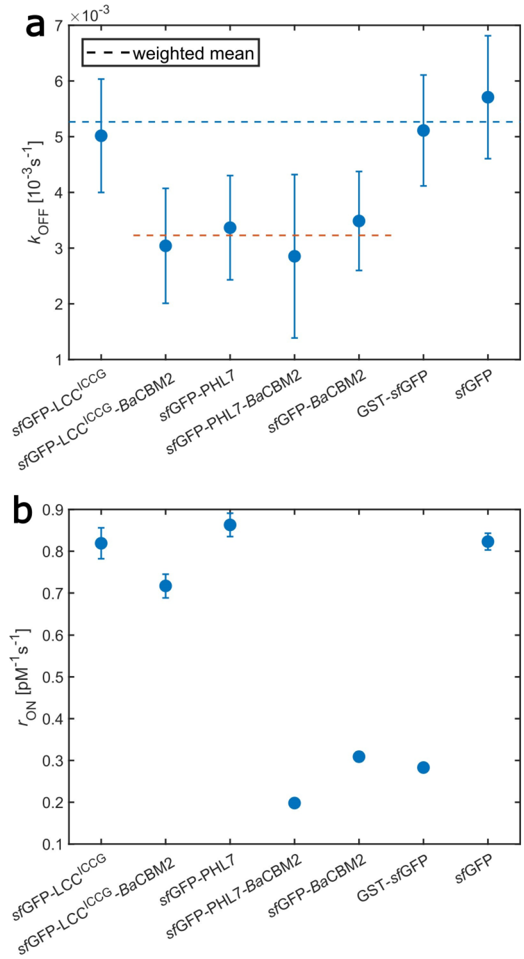

Figure 4. Kinetics of PET hydrolases. a) k_{OFF} calculated as the inverse of the residence time for each enzyme. The enzymes exhibit differences in the dissociation constant. Error bars are propagated from the error on fitting parameters of individual residence time histograms. The dashed lines represent the weighted mean of each group of proteins. b) The molar binding rate constant r_{ON} for each protein, revealing differences in their binding kinetics. Error bars correspond to the s.e.m.

Table 2. Dissociation rate constants and binding rate constants for each protein calculated based on TIRF microscopy data.

Protein	k_{OFF} ($10^{-3}\ s^{-1}$)	r_{ON} ($pM^{-1}\ s^{-1}$)
*sf*GFP-LCC^{ICCG}	5 ± 1	0.819 ± 0.037
*sf*GFP-LCC^{ICCG}-*Ba*CBM2	3 ± 1	0.717 ± 0.027
*sf*GFP-PHL7	3 ± 1	0.863 ± 0.028
*sf*GFP-PHL7-*Ba*CBM2	3 ± 1	0.198 ± 0.007
*sf*GFP-*Ba*CBM2	3 ± 1	0.309 ± 0.011
GST-*sf*GFP	5 ± 1	0.283 ± 0.020
*sf*GFP	6 ± 1	0.823 ± 0.023

*sf*GFP-*Ba*CBM2 exhibiting a much slower binding ($r_{ON} = 0.198 \pm 0.007$ pM^{-1} s^{-1} and $r_{ON} = 0.309 \pm 0.011$ pM^{-1} s^{-1}, respectively) than their analogs without the binding module ($r_{ON} = 0.863 \pm 0.028$ pM^{-1} s^{-1} and $r_{ON} = 0.823 \pm 0.020$ pM^{-1} s^{-1}, respectively), as is depicted in Figure 3b.

It should be acknowledged that the obtained r_{ON} values in this study should not be confused with the k_{ON} rate constant. In this context, r_{ON} is defined as the product of N, representing the number of binding sites probed within the Field-of-View (FOV), and k_{ON}, which denotes the molar association rate constant. The number of binding sites available in the Field-of-View, N, can not be readily calculated in assays where the substrate is deposited on a surface, like ours. In this study, it was ensured that the PET film was continuous, covering the full extent of each Field-of-View during experimentation, thereby maintaining an equal surface area of the PET film, and hence a constant N for all measurements. Therefore, it can be assumed that the changes in the binding rates observed reflect changes of each enzyme's k_{ON}.

Despite variations in the value of N (Figure 3b), the number of new tracks starting at each frame of the time-lapse series, the analysis demonstrates that the dataset is aptly represented by its mean. This assertion is corroborated by the alignment of the mean with the bulk of the error bars. Further substantiation comes from a chi-square test, which produced a p-value exceeding 0.05. Such a result suggests the absence of significant discrepancies between the observed data and the anticipated distribution, endorsing the mean as an appropriate descriptor for our dataset. Consequently, both the standard deviation and the standard error of the mean are minimal, indicating a tight clustering of the data points around the mean. This observation solidifies the statistical integrity and well-defined character of the calculated r_{ON} in our study.

Lastly, we emphasize that the steady-state binding data (Table 1) primarily serves to illustrate the high affinity of the proteins for PET, and drawing direct comparisons with TIRF experiments is challenging due to differing theoretical bases and concentration disparities exceeding three orders of magnitude. In TIRF, only the most favorable binding sites are engaged at very low concentrations, whereas steady-state experiments measure an average binding across all sites on a saturated surface. Additionally, the binding rate constant r_{ON}, calculated in relation to enzyme concentration, differs from the k_{ON} association rate constant, which is based on the concentration of binding sites. Hence, comparing these binding data directly with kinetic data from bulk assays, where substrate concentration is uniform, would not yield accurate results.

Table 3. Results from FRAP assays on amorphous PET discs incubated with *sf*GFP-labelled proteins of various concentrations. Recovery half-time ($t_{1/2}$) (s^{-1}) (top) and mobile fraction (M_f) (%) (bottom). Values are the mean of three replicates, standard deviations are given. A "–" symbol indicates little or no recovery observed during the time course of the FRAP experiments. Individual normalised recovery curves can be found in Figures S6–S9.

Concentration of enzyme	1000 nM	500 nM	100 nM
	$t_{1/2}$ (s^{-1})		
sf GFP-LCC^{ICCG}	5.30 ± 0.11	4.89 ± 0.79	–
*sf*GFP-LCC^{ICCG}-*Ba*CBM2	5.07 ± 1.62	–	–
*sf*GFP-PHL7	6.84 ± 1.38	5.06 ± 0.45	–
*sf*GFP-PHL7-*Ba*CBM2	6.31 ± 1.11	–	–
*sf*GFP-*Ba*CBM2	–	–	–
*sf*GFP	5.11 ± 1.43	4.37 ± 0.24	–
	M_f (%)		
*sf*GFP-LCC^{ICCG}	91.0 ± 13.2	82.0 ± 3.4	–
*sf*GFP-LCC^{ICCG}-*Ba*CBM2	86.0 ± 13.5	–	–
*sf*GFP-PHL7	43.0 ± 5.2	63.0 ± 4.9	–
*sf*GFP-PHL7-*Ba*CBM2	31.0 ± 0.9	–	–
*sf*GFP-*Ba*CBM2	–	–	–
*sf*GFP	97.0 ± 7.3	91.0 ± 0.9	–

FRAP Microscopy

FRAP microscopy was done with the exact same enzymes as studied by TIRF, to measure dynamic rates of movement of proteins in these systems (Figure 1f and Figure 5). The results for recovery half-time $t_{1/2}$, and mobile fraction (M_f) measured in FRAP experiments are outlined in Table 3. When recovery was observed, the $t_{1/2}$ values consistently fell within the range of 4 to 7 seconds. This is in contrast to the r_{ON} rates measured by TIRF microscopy, which were in the order of 0.1–1 pM^{-1} s^{-1} (Figure 4). Given that the concentrations used in these experiments, and in most cases of PET hydrolysis, is in the range of hundreds or thousands of nM, then it would be expected that off rates are the dominant factor in the protein dynamics at the PET surface. It is therefore assumed that the $t_{1/2}$ measured in FRAP experiments on these systems is functionally equal to k_{OFF}, with each enzyme therefore having a k_{OFF} in the region of 10^{-3} s^{-1}. It is important to note that the difference in k_{OFF} values observed in TIRF and FRAP experiments is several orders of magnitude, in comparison to $t_{1/2}$. This discrepancy suggests the possibilty of a more complex dynamic system in the FRAP experiments, where k_{OFF} is not the sole determining factor. However, this difference could be attributed to the large disparity in enzyme concentrations used in the two experiments. TIRF, being a single-molecule technique, involves imaging at low pM concentrations of enzyme, while the FRAP assays were conducted at concentrations ranging from 100 nM to 1000 nM. It is known that a PET surface exhibits heterogeneity in terms of enzyme binding.[29] This heterogeneity will lead to enzymes occupying the most stable binding sites at low protein concentrations. This could explain the considerably slower k_{OFF} values in the TIRF experiments, as the best binding sites occupied at these low concentrations would necessarily have a slower k_{OFF}. Additionally, the variation in k_{OFF} maybe ascribed to the occurrence of multi-layer adsorption on the surface at the significantly higher concentrations used in

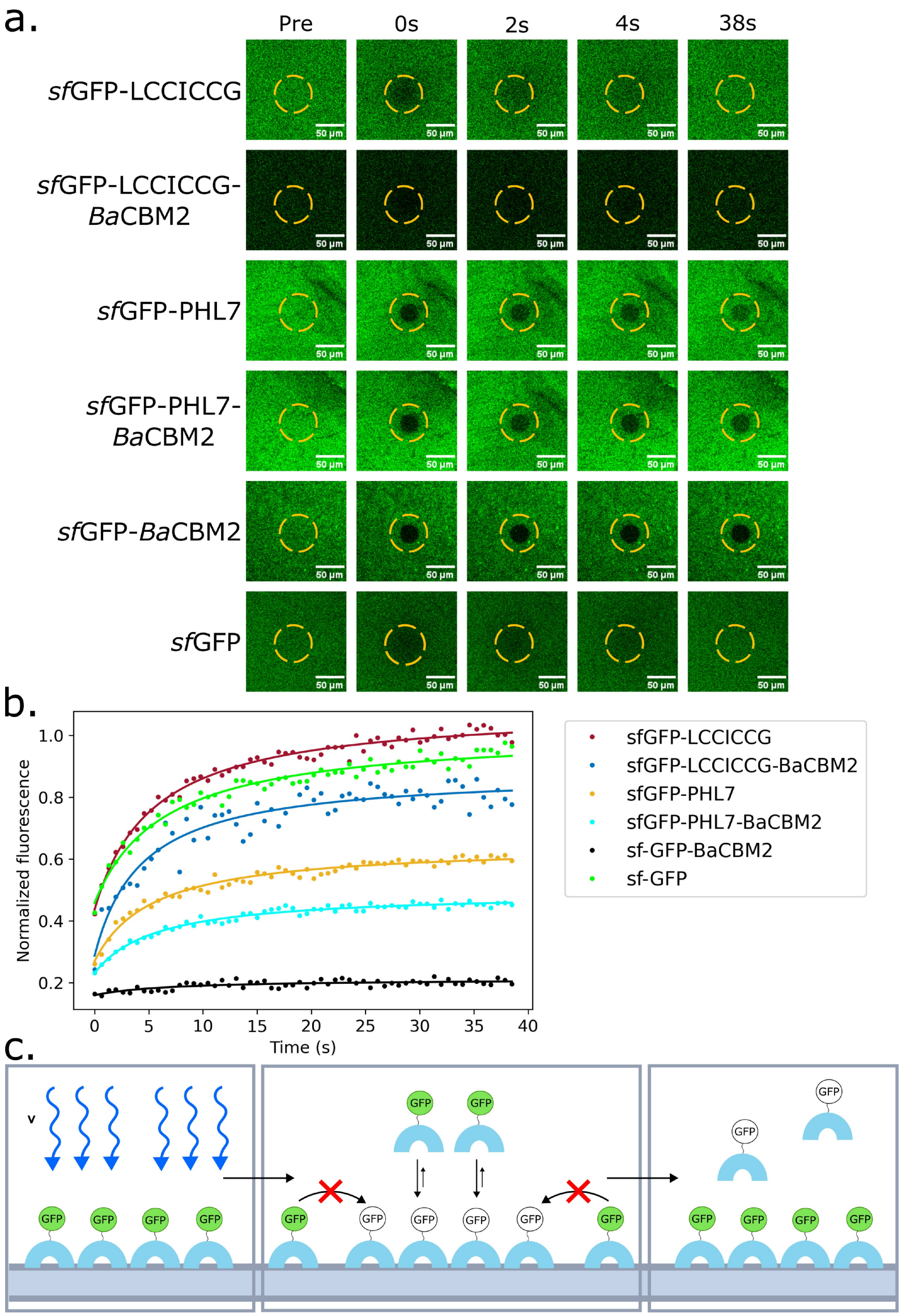

Figure 5. Fluorescence Recovery After Photobleaching (FRAP) experiments on an amorphous PET disc. a) Snapshots of a representative single replicate of the FRAP experiments. The Pre-bleach is taken as the final frame before bleaching, with the timepoint of every frame shown above the figures. The final frame in each experiment is at 38 seconds. The bleaching region is indicated by a circle. b) Comparison of the normalized FRAP curves of single representative replicates from all of the proteins assayed in the 1000 nM incubation experiments. c) A schematic of the proposed model for the dynamics of PET hydrolases at the PET surface. Recovery rates during the FRAP experiments are dominated by the relatively slow off rates compared to the faster on rates. Lateral diffusion over the surface is considered negligible.

the FRAP experiments. This challenges the monolayer assumption made in the modelling of each system.

The addition of the *Ba*CBM2 module to both LCC^{ICCG} and PHL7 seems to have altered the dynamics of the proteins at the PET surface during the FRAP experiments. No recovery was seen by neither *sf*GFP-LCC^{ICCG}-*Ba*CBM2 nor *sf*GFP-PHL7-*Ba*CBM2, when the PET discs were incubated with 500 nM of protein, compared to the analogous constructs without *Ba*CBM2. This suggests that the binding of *Ba*CBM2 is much more stable than the other modules within these constructs, as the bleached molecules containing the binding module are much less mobile during these time scales. Furthermore, no recovery was seen at any concentration when *sf*GFP-*Ba*CBM2 was assayed, which again demonstrates the strong specific binding of this module, compared to the transient weaker binding demonstrated by the PET hydrolase modules. These result clearly show that the addition of a CBM greatly affects the dynamics of proteins at the PET surface.

Lateral Diffusion Assays Using FRAP Microscopy

Many of the FRAP studies of protein surface dynamics with substrates such as cellulose make the assumption that recovery is driven by lateral diffusion of the enzymes over the surface.[22,30] While this assumption could be considered valid for cellulases, as processive activity is a well-known feature of many of these enzymes,[31,32] it remains uncertain whether this property extends to PET hydrolases on a PET surface. The rapid recovery observed over a short period of time in the FRAP experiments has led to the proposal of two models for PET hydrolase dynamics: i) Lateral diffusion occurs over the surface of the PET, resulting in the recovery of the fluorescent signal; ii) Dynamics are predominantly governed by the desorption of bleached enzymes, followed by the subsequent adsorption of fresh enzyme from the bulk solution. To study this, we designed an experiment where PET discs were pre-incubated with 1000 nM of enzyme, washed, and placed in a fresh well containing buffer without free enzyme. The recovery period for these experiments was extended to 20 minutes, compared to the 40 seconds in the experiments described above, ensuring any slower recovery could be detected over longer periods. The experiment was performed with a lower imaging frequency to prevent enzyme bleaching over this extended period. None of the constructs showed significant recovery over the 20 minute period (Figure S8 and Figure S9). The absence of recovery in experiments without free protein in the bulk solution seems to rule out the possibility of lateral diffusion, thereby supporting the second model, where recovery is predicated by desorption and adsorption on the PET surface. This conclusion is further reinforced by the lack of recovery on discs incubated with 100 nM of enzyme, a concentration within the region of K_d of each enzyme (Table 1), indicating incomplete saturation under these conditions. If lateral diffusion was occurring significantly, it would also be expected that unbleached enzyme would diffuse into unsaturated areas on the disc from outside the ROI. As this is not seen we conclude that lateral diffusion is negligible in these systems, with dynamics primarily dominated by adsorption and desorption.

One of the major questions when modelling the degradation of PET by these enzymes is that of processivity. The results of the TIRF experiments suggest that PET hydrolases spend enough time on a PET surface to hydrolyse a number of bonds, given that the enzyme turnover number (k_{cat}) of LCC^{ICCG} is approximately 0.3 s^{-1} under relevant conditions.[14] However, the non-specific binding model suggested based on the TIRF data in this study would support the conclusion that the majority of enzymes bound to the surface of PET do not exhibit processive behavior. Furthermore, the results from the FRAP experiments indicate negligible lateral diffusion over the PET surface, as discussed below. Overall, therefore, the data in this study do not seem to support processivity of PET hydrolases during hydrolysis.

Conclusions

In this study, a TIRF microscopy methodology has been developed that is specifically suited to use with a PET substrate and *sf*GFP labeled proteins. This has allowed single-molecule tracking of both *sf*GFP-LCC^{ICCG} and *sf*GFP-PHL7 at a PET surface. The k_{OFF} and r_{ON} of each protein was measured, and found to be similar to non-productive binding of other proteins to insoluble hydrophobic substrates. The k_{OFF} and r_{ON} values of these proteins have not been previously measured in these systems, and this method can be applied to analyse enzyme variants designed to optimize these factors for increased enzyme efficiency.

The FRAP microscopy analysis showed that *sf*GFP-LCC^{ICCG} had a much higher protein motility than *sf*GFP-PHL7, which on the other hand had a larger stationary fraction. This can be used to explain the differences in activity of these two enzymes. The recovery rates were also found to be highly dependent on the concentration of free enzyme. This led to a potential model in which the exchange on the surface is dominated by the slow k_{OFF} rates as measured using TIRF microscopy, rather than any lateral diffusion of the proteins over the surface. This has not been discussed before in the context of enzymatic PET hydrolysis, and it is an important result in the understanding of enzyme dynamics in these systems. It was also shown that fusion of a CBM to the enzymes severely impedes the dynamics of these enzymes on a PET surface.

The development of these two methods for assessing the dynamics of PET hydrolases at a PET surface expands the toolbox available to researchers for further advancements in engineering these enzymes. The results and insights on dynamic models represent significant advancement in our understanding of these enzymes, and can be used in further development of enzymatic recycling of PET.

Experimental Section

Materials

The PET substrate used in this study was obtained from Goodfellow (UK). Specifically, a 0.25 mm-thick sheet of amorphous PET (Product code: ES30-FM-000145) was cut into 6 mm-diameter discs, using a hand punch. These were then used for the activity and binding assays. Additionally, these discs were used in the FRAP experiments. For the TIRF experiments, a drop-cast PET film, produced in house as described below, was used. A commercial GST-GFP protein (Protean, Czechia) was purchased for use as a control in the TIRF experiments.

Strains and constructs

Protein expressions were carried out in *Escherichia coli* BL21(DE3). All genes for enzyme expression were synthesized by GenScript (USA) and subcloned into the pET-21b(+) vector. All constructs were designed with a 6xHis purification tag at the N-terminus, followed by the *sf*GFP module (Genbank accession: ASL68970). The LCC^{ICCG} (Genbank accession: HQ704839) and PHL7 (Genbank accession: LT571446) catalytic domains were then fused to the C-terminus of the *sf*GFP module. The *Ba*CBM2 module (Genbank accession: ACQ50287) was fused to the C-terminus of the catalytic domains. Residues 459 to 484 from *Trichoderma reesei* Cel7A (Genbank accession: P62694) were used as a linker to connect each of the domains. Analogous constructs without the sfGFP module were also produced for comparison of enzyme activity. A construct was also produced with the *Ba*CBM2 linked directly to the C-terminus of *sf*GFP, however in this case, a (GS)×5 linker was used. Each of the fusion proteins also had a StrepII tag (WSHPQFEK) at the C-terminus. These were designed into the constructs as a secondary purification tag, which was not required during our purifications. The primary sequences of each construct can be found in the Supporting Information note N1.

Enzyme expression and purification

10 mL of LB medium with 100 μg/L of ampicillin was inoculated with single clones of *E. coli* cells harboring the relevant plasmid, and grown overnight at 37 °C, 200 rpm. This overnight culture was used to inoculate 750 mL of LB medium in 3 L shake flasks, to an approximate OD_{600} of 0.1. These were then incubated at 37 °C, 160 rpm until the OD_{600} reached 0.6–0.8. At this point, temperature was reduced to 16 °C, and the expression was induced with Isopropyl β-D-1-thiogalactopyranoside (IPTG) to a final concentration of 0.1 mM. The culture was then left to grow for 18 hours. The cells were harvested by centrifugation at 4000 *g* for 30 minutes at 4 °C, and the resulting cell pellet was stored at −20 °C until purification.

A cell pellet was resuspended in binding buffer (10 mM HEPES, 500 mM NaCl, 10 mM imidazole, 10% glycerol, pH 7,5) with an added protease inhibitor tablet (Roche, Switzerland) and lysed by sonication. Following addition of Benzonase nuclease (Thermofisher, USA) the cell debris was separated by centrifugation at 40,000 *g* for 30 minutes at 4 °C. The supernatant was filtered through a 0.45 μm filter, and loaded on a His-Trap FF 5 mL column (Cytiva, USA) preequilibrated with binding buffer. The column was washed with 15 mL of binding buffer, and then the protein was eluted with three steps of 15 mL binding buffer containing 40 mM, 240 mM and 400 mM of imidazole, respectively. The fraction containing a visible GFP signal was then applied to a Superdex 16/60, 200 pg size exclusion column on an Akta Avant (Cytiva, USA) chromatography system using a storage buffer (10 mM HEPES, 150 mM NaCl, 10% glycerol, pH 7.5). For purification of constructs lacking the (*sf*GFP) module, the 240 mM imidazole fraction was applied to the size exclusion column. Any buffer exchanges were performed by overnight dialysis using a 3.5 kDa MWCO standard dialysis tubing (Spectrum Labs, USA). Protein concentration was determined using absorbance at 280 nm and the theoretical extinction coefficients.

Activity assays

The activity of the enzymes was quantified using a modified version of the assay previously described.[33] In short, single amorphous PET discs were added to low-binding Eppendorf tubes, and incubated in 500 μL assay buffer (50 mM phosphate, pH 8.0) containing 300 nM enzyme. The tubes were incubated at 65 °C and 1000 rpm for 3 hours, and the soluble products were detected in 100 μL of reaction media in a UV-star 96-well plate at 240 nm using a spectrophotometer (Thermofisher, USA). A standard curve was made using Bis(2-Hydroxyethyl) terephthalate (BHET), and activity was reported as BHET equivalents.

Binding assays

Bulk affinity of each *sf*GFP labeled protein was quantified using the assay previously described.[23] In short, discs of amorphous PET were placed in a low protein binding 96-well plate, and washed in succession with 10% SDS and deionized water. The discs were then incubated in storage buffer for 30 minutes, before protein was added in a titration series between 50 nM and 1000 nM. The plate was then incubated at 20 °C and 300 rpm for 60 minutes in a thermomixer (Eppendorf, Germany). Following this, the liquid in each well was moved to a fluorescence-suitable 96-well plate and the concentration of unbound protein was determined using a FP-8500 spectrofluorimeter equipped with an FMP-825 plate reader (JASCO Corporation, Japan) with excitation at 450 nm and emission at 510 nm. Standard curves of each protein were prepared by adding protein to wells without substrate and treating standards with the exact conditions as the samples before moving them to neighboring wells. The amount of protein bound to each disc was calculated by subtracting the unbound from the total protein added and dividing by the surface area of the disc, and the dissociation constant K_d was determined by fitting the binding isotherm described in Eq. (1):

$$[BP] = \frac{[FP][BP]_{max}}{K_d + [FP]} \tag{1}$$

where [BP] and [FP] are the concentrations of bound and free protein, respectively. A minimum of seven protein concentrations were used to produce each binding isotherm for K_d determinations.

Glass surface preparation

For TIRF experiments, a glass-bottomed μ-Slide was utilized (Ibidi GmbH, Munich, Germany, catalog number 80827). Due to the plates' open wells, they provide the possibility to add/remove solutions at any time during experimentation. For example, photobleaching of the PET surface was performed in buffer, which was then removed before the enzyme solution was added. To ensure optimal conditions for single-molecule imaging, we took meticulous steps to clean the wells and eliminate potential sources of background noise: The cleaning procedure involved sonication using Triton-X100 and KOH, as described elsewhere.[34]

Drop casting of PET

Four amorphous PET discs were added to 1 mL of hexafluoroisopropanol (HFIP) and left overnight to dissolve. The resulting solution was filtered through a 0.22 μm PES syringe filter, and diluted 1:10 in HFIP. 7 μL was added to each well of the prepared well-plate, and was allowed to dry in a LAF bench.

TIRF microscopy

An inverted Nikon TiU microscope modified with a homemade objective-based total internal reflection fluorescence (TIRF) module was used for imaging.[35] An Electron-Multiplying Charge-Coupled Device (EMCCD) camera (Evolve 512, Photometrics) and a quad-band filter cube (AHF, TIRF quad HC Ex. 390/482/532/640, Em. 446/523/600/677) were employed. The microscope used a 100×/1.45 oil objective, and an intermediate magnification lens was utilized, resulting in a total magnification of 150×, corresponding to a pixel size of 107 nm. Our field-of-view covered an area of 54×54 μm^2.

For imaging the different enzyme constructs, a 473 nm-laser line was used at a power of 2 mW, resulting in an estimated power density of 93 W/cm^2. The exposure time was set to 100 ms. The EMCCD camera electron-multiplying (EM) gain was calibrated to 44 counts per photon for an EM Gain of 500 and a camera gain of 3.[36]

TIRF microscopy procedure

To ensure proper focusing, the autofluorescence of the PET film in the red channel (at 638 nm excitation) was employed for autofocusing in MicroManager[37] every 10 frames. During refocusing, imaging conditions for the autofluorescence were adjusted so that the illumination dose was minimized: excitation at 638 nm was lowered to 1.2 mW, exposure time was reduced to 20 ms, and there was no camera gain or EM-gain.

Before the start of the experiment, the optimal TIR angle was determined by adjusting the motorized mirror until fluorescence background from the solution drops. During the experiment, the TIR angle was readjusted whenever the field of view was moved over the sample. All experiments were conducted at a temperature of 20 °C.

For each experimental condition a time-lapse movie of 500 frames (approximately 10 minutes) was recorded. Before image acquisition, the area of interest on the PET was bleached using 5 mW of power for 1 minute to minimize the autofluorescence in the green emission channel. This was done prior to the addition of protein to the well. After acquisition, we changed the well and repeated the process of bleaching and image acquisition. For for fluorophore lifetime extension, we degassed the buffer and utilized a Nitrogen flow over the well-plate to prevent molecular oxygen from diffusing back in the sample. We did not use other techniques such as enzymatic oxygen scavenging systems due to the mismatch of pH between our enzymes and typical pH range of those systems.

*sf*GFP bleaching assay

10 μg/mL BSA (thermoFisher, USA) was mixed with 1 μg/mL BSA-Biotin (Eurogentec, Belgium) in a 100:1 ratio, and 300 μL added to a well in a cleaned Ibidi slide. After a 20 minute incubation, the solution was removed and the well was then washed 1 times with 1×Tris-EDTA buffer. 300 μL of 0.5 μg/mL Streptavidin (ThermoFisher, USA) was then added to the wells, followed by another 1 times wash 1×Tris-EDTA buffer. 300 μL of storage buffer containing 0.05 μg/mL of the *sf*GFP-*Ba*CBM2 protein, with the StrepII tag on the C-terminus, was added to the wells, and allowed to bind for 10 minutes, followed by another wash to remove unbound protein. A region was then subjected to the same conditions as used in the TIRF binding experiments (see section TIRF microscopy procedure), and the fluorescence imaged over a period of 500 seconds. Green fluorescing fiducial markers (FisherScientific, 140 nm) were used to account for microscope drift and autofocus. As they fluoresce in the same channel as *sf*GFP but remain on for the entire duration of the movie, they were excluded from the analysis.

Processing of TIRF microscopy data

We used the TrackMate[38] plugin in Fiji to track individual fluorescence spots in time-lapse movies captured through Total Internal Reflection Fluorescence microscopy (TIRF). Filters and detection parameters were adjusted to obtain a robust detection of single molecule spots in the TIRF images (see Supporting Information for further details).

The spot lifetime was measured from the time a spot first detected. Spots already present on the first frame and those still present at the last frame of a movie were excluded from the analysis as it would be impossible to assess the full extend of their lifetime. To assess the rate of binding, we calculated the number of tracks starting at each frame, for every frame in the time-lapse. The resulting count was then divided by the frame interval of 1 second. To calculate the molar binding rate, we divided by the concentration of enzyme used (10 pM).

For a single time-lapse movie, we analyzed the lifetime histogram by fitting it with a double exponential decay model. The error associated with the characteristic lifetime was determined from the covariance matrix of the fit. To determine the residence time and the corresponding k_{OFF} (dissociation rate constant), we considered the photobleaching of the fluorophore. We accounted for the error in the lifetime measurement and the bleaching time, propagating them to obtain the error reported for the k_{OFF} values in individual time-lapse movies.

FRAP microscopy

Amorphous PET discs were incubated with *sf*GFP labelled proteins in 500 μL at 100 nM, 500 nM, or 1000 nM overnight at 4 °C with gentle shaking. The dics were then added to a 96-well PhenoPlate with a glass bottom suitable for fluorescence microscopy. Then the supernatant from the overnight saturation was added to the well with the disc. For the lateral diffusion assays, the discs were preincubated with 1000 nM of protein overnight and then washed three times with storage buffer before being added to the well with fresh storage buffer. Imaging was performed on a Leica (Germany) SP8 confocal microscope, at a magnification of 20×. Initially, focusing was done using the white light channel to focus on the surface of the disc, with the *sf*GFP labelled proteins imaged with the 488 nm laser at a gain of 1250 V. For the bleaching, a circular area with a 28×28 μm dimension was designated as the region of interest (ROI), which was then imaged at 1% laser power for 5 frames of 650 ms pre-bleach, then bleached at 100% power for 10 frames of 605 ms. Recovery was then imaged at 1% power for 100 frames of 650 ms. Two additional ROIs were also imaged corresponding to the background signal in a region without a fluorescent signal, and a fluorescent active region corresponding to an unbleached region. The data analysis was then performed following the method described by Day *et al.*[39] The fluorescent signal was normalised by using the following equation:

$$F(t)_{\text{norm}} = \frac{F(t)_{\text{ROI}} - F_{\text{bckgd}}}{F(t)_{\text{Disc}} - F_{\text{bckgd}}} \times \frac{F(i)_{\text{Disc}} - F_{\text{bckgd}}}{F(i)_{\text{ROI}} - F_{\text{bckgd}}} \tag{2}$$

Where $F(t)_{\text{ROI}}$ is the signal in the bleached area at each timepoint, $F(t)_{\text{Disc}}$ is the unbleached signal at each timepoint, $F(i)_{\text{ROI}}$ is the fluorescent signal in the bleaching area on the frame prior to bleaching, $F(i)_{\text{Disc}}$ is the signal from the unbleached area on the frame prior to bleaching, and F_{bckgd} is the signal from a region without any *sf*GFP labelled protein. This normalised signal was then plotted against time, with the first frame after bleaching being set as $t=0$ s. The rate of recovery was then quantified by calculating half times of recovery ($t_{1/2}$) using the following equation:

$$F(t) = \frac{F_0 + F_\infty \left(t/t_{1/2}\right)}{1 + \left(t/t_{1/2}\right)} \tag{3}$$

Where F_0 and F_∞ are the fluorescent signals immediately after the bleach, and after full recovery (at the asymptote). $t_{1/2}$ is reported for each protein in units of reciprocal seconds.

The percentage of molecules mobile enough to allow recovery, known as the mobile fraction (M_f), was then calculated using the following equation:

$$M_f = \frac{F_\infty - F_0}{F(i)_{\text{ROI}} - F_0} \times 100 \tag{4}$$

Mobile fraction was expressed as a percentage for each protein. Each FRAP assay was performed in triplicate in different regions of the same disc, which had been incubated overnight with 100, 500, or 1000 nM of protein. An experiment was also performed in which a disc was incubated with 1000 nM of each particular protein overnight, washed with storage buffer three times, and then placed in a well with buffer. A single FRAP experiment was then performed on these washed discs with the same pre-bleach and bleaching conditions, however the post-bleach recovery phase was run for 250 frames of 5 seconds each.

Acknowledgements

The authors thank Claus Sternberg for his assistance in operation of the confocal microscope in the FRAP experiments, Rasmus Greve Falbe-Hansen for assistance in handling the FRAP data, Pedro Rodrigues and Mette Christine Nørgaard Kejlstrup for their help in purification of the enzymes, and Anne Meyer for kindly providing the plasmids used in the gene expression. The authors also wish to acknowledge funding from Novo Nordisk Foundation (grant NNF19OC0055625) for the infrastructure “Imaging microbial language in biocontrol (IMLiB)“. Research reported in this publication is supported by the Novo Nordisk Foundation Biotechnology-based Synthesis and Production programme, under the grant number NNF19OC0057587 (RM, AN, PW) and The Danish Independent Research Council (DFF) [grant number: 1032-00273B] (AR, MSM, PW).

Conflict of Interests

The authors declare no conflicts of interest.

Data Availability Statement

The data that support the findings of this study are available from the corresponding author upon reasonable request.

Keywords: enzyme catalysis · fluorescence microscopy · green chemistry · interfacial catalysis · PET hydrolases · surface dynamics

[1] G. M. Guebitz, A. Cavaco-Paulo, *Trends Biotechnol.* **2008**, *26*, 32.
[2] C. M. Carr, D. J. Clarke, A. D. Dobson, *Front. Microbiol.* **2020**, *11*, 571265.
[3] F. Kawai, T. Kawabata, M. Oda, *ACS Sustainable Chem. Eng.* **2020**, *8*, 8894.
[4] V. Tournier, C. Topham, A. Gilles, B. David, C. Folgoas, E. Moya-Leclair, E. Kamionka, M.-L. Desrousseaux, H. Texier, S. Gavalda, et al., *Nature* **2020**, *580*, 216.
[5] S. Sulaiman, S. Yamato, E. Kanaya, J.-J. Kim, Y. Koga, K. Takano, S. Kanaya, *Appl. Environ. Microbiol.* **2012**, *78*, 1556.
[6] C. Sonnendecker, J. Oeser, P. K. Richter, P. Hille, Z. Zhao, C. Fischer, H. Lippold, P. Blázquez-Sánchez, F. Engelberger, C. A. Ramírez-Sarmiento, et al., *ChemSusChem* **2022**, *15*, e202101062.
[7] A. Rennison, J. R. Winther, C. Varrone, *Polymer* **2021**, *13*, 3884.
[8] P. K. Richter, P. Blázquez-Sánchez, Z. Zhao, F. Engelberger, C. Wiebeler, G. Künze, R. Frank, D. Krinke, E. Frezzotti, Y. Lihanova, et al., *Nat. Commun.* **2023**, *14*, 1905.
[9] J. D. Nill, T. Jeoh, *ACS Sustainable Chem. Eng.* **2020**, *8*, 6722.
[10] D. Ribitsch, A. O. Yebra, S. Zitzenbacher, J. Wu, S. Nowitsch, G. Steinkellner, K. Greimel, A. Doliska, G. Oberdorfer, C. C. Gruber, et al., *Biomacromolecules* **2013**, *14*, 1769.
[11] D. Ribitsch, E. Herrero Acero, A. Przylucka, S. Zitzenbacher, A. Marold, C. Gamerith, R. Tscheließnig, A. Jungbauer, H. Rennhofer, H. Lichtenegger, et al., *Appl. Environ. Microbiol.* **2015**, *81*, 3586.
[12] S. F. Badino, J. A. Bååth, K. Borch, K. Jensen, P. Westh, *Enzyme Microb. Technol.* **2021**, *152*, 109937.
[13] J. Arnling Bååth, V. Novy, L. V. Carneiro, G. M. Guebitz, L. Olsson, P. Westh, D. Ribitsch, *Biotechnol. Bioeng.* **2022**, *119*, 470.
[14] J. Arnling Bååth, K. Jensen, K. Borch, P. Westh, J. Kari, *JACS Au* **2022**, *2*, 1223.
[15] R. Graham, E. Erickson, R. K. Brizendine, D. Salvachúa, W. E. Michener, Y. Li, Z. Tan, G. T. Beckham, J. E. McGeehan, A. R. Pickford, *Chem. Catal.* **2022**, *2*, 2644.
[16] D. Axelrod, *J. Cell Biol.* **1981**, *89*, 141.
[17] A. R. Mudinoor, P. M. Goodwin, R. U. Rao, N. Karuna, A. Hitomi, J. Nill, T. Jeoh, *Biotechnol. Biofuels* **2020**, *13*, 1.
[18] Y.-S. Liu, Y. Luo, J. O. Baker, Y. Zeng, M. E. Himmel, S. Smith, S.-Y. Ding, A single molecule study of cellulase hydrolysis of crystalline cellulose, in *P. Soc. Photo-Opt. Ins*, vol. 7571, SPIE **2010**, pages 9–16.
[19] Z. K. Haviland, D. Nong, K. L. V. Kuntz, T. J. Starr, D. Ma, M. Tien, C. T. Anderson, W. O. Hancock, *J. Biol. Chem.* **2021**, *297*, 101029.
[20] D. Nong, Z. K. Haviland, M. Mayers, M. Tien, C. T. Anderson, W. O. Hancock, *Biophys. J.* **2022**, *121*, 423a.
[21] Y. Shibafuji, A. Nakamura, T. Uchihashi, N. Sugimoto, S. Fukuda, H. Watanabe, M. Samejima, T. Ando, H. Noji, A. Koivula, et al., *J. Biol. Chem.* **2014**, *289*, 14056.
[22] E. J. Jervis, C. A. Haynes, D. G. Kilburn, *J. Biol. Chem.* **1997**, *272*, 24016.
[23] A. P. Rennison, P. Westh, M. S. Møller, *Sci. Total Environ.* **2023**, *870*, 161948.
[24] M. Koida, H. Nakamuta, J. Mayuso, Y. Yamamoto, *Jpn. J. Pharmacol.* **1982**, *32*, 413.
[25] M. Goebel-Stengel, A. Stengel, Y. Taché, J. R. Reeve Jr, *Anal. Biochem.* **2011**, *414*, 38.
[26] A. B. Boraston, D. N. Bolam, H. J. Gilbert, G. J. Davies, *Biochem. J.* **2004**, *382*, 769.
[27] T. B. Thomsen, S. Schubert, C. J. Hunt, K. Borch, K. Jensen, J. Brask, P. Westh, A. S. Meyer, *ChemSusChem* **2023**, *16*, e202300291.
[28] J. Jung, A. Sethi, T. Gaiotto, J. J. Han, T. Jeoh, S. Gnanakaran, P. M. Goodwin, *J. Biol. Chem.* **2013**, *288*, 24164.
[29] T. B. Thomsen, K. Almdal, A. S. Meyer, *New Biotechnol.* **2023**.
[30] J. M. Moran-Mirabal, J. C. Bolewski, L. P. Walker, *Biotechnol. Bioeng.* **2013**, *110*, 47.
[31] D. B. Wilson, M. Kostylev, *Biomass Convers.* **2012**, pages 93–99.

[32] K. Zajki-Zechmeister, G. S. Kaira, M. Eibinger, K. Seelich, B. Nidetzky, *ACS Catal.* **2021**, *11*, 13530.
[33] E. Z. L. Zhong-Johnson, C. A. Voigt, A. J. Sinskey, *Sci. Rep.* **2021**, *11*, 928.
[34] B. E. Snaar-Jagalska, A. Cambi, T. Schmidt, S. D. Keijzer, *Single-molecule imaging technique to study the dynamic regulation of gpcr function at the plasma membrane*, vol. 521, Elsevier Inc., 1 edition **2013**.
[35] A. C. Hundahl, A. Weller, J. B. Larsen, C. U. Hjørringgaard, M. B. Hansen, A.-K. Mündler, A. Knuhtsen, K. Kristensen, E. C. Arnspang, T. L. Andresen, et al., *J. Controlled Release* **2023**, *355*, 122.
[36] K. I. Mortensen, H. Flyvbjerg, *Sci. Rep.* **2016**, *6*, 1.
[37] A. D. Edelstein, M. A. Tsuchida, N. Amodaj, H. Pinkard, R. D. Vale, N. Stuurman, *J. Microbiol. Methods* **2014**, *1*, e10.
[38] D. Ershov, M.-S. Phan, J. W. Pylvänäinen, S. U. Rigaud, L. Le Blanc, A. Charles-Orszag, J. R. Conway, R. F. Laine, N. H. Roy, D. Bonazzi, et al., *Nat. Methods* **2022**, *19*, 829 .
[39] C. A. Day, L. J. Kraft, M. Kang, A. K. Kenworthy, *Curr. Protoc. Cytom.* **2012**, *62*, 2.

Manuscript received: September 27, 2023
Revised manuscript received: December 21, 2023
Accepted manuscript online: January 15, 2024
Version of record online: February 12, 2024